# Multi-Conductor Transmission Line Networks in Analysis of Side-Coupled Metal-Insulator-Metal Plasmonic Structures

Ali Eshaghian, Meisam Bahadori, Mohsen Rezaei, Amin Khavasi, Hossein Hodaei, and Khashayar Mehrany*

*Department of Electrical Engineering, Sharif University of Technology, Tehran 11155–4363, Iran*

**Corresponding author: mehrany@sharif.edu*

**Abstract**

An approximate and accurate enough multi-conductor transmission line model is developed for analysis of side-coupled metal-insulator-metal (MIM) waveguides. MIM waveguides have been already modeled by single conductor transmission lines. Here, the side coupling effects that exist between neighboring plasmonic structures are taken into account by finding appropriate values for distributed mutual inductance and mutual capacitance between every two neighboring conductors in the conventional single-conductor transmission line models. In this manner, multi-conductor transmission line models are introduced. Closed-form expressions are given for the transmission and reflection of miscellaneous MIM plasmonic structures, e.g. dual-stop-band and band-pass filters. In all examples, the results of the proposed model are compared against the fully numerical finite-difference time-domain (FDTD) method. The results of the analytical model are in good agreement with the numerical results.

*Keywords:* Distributed circuits, Optical filters, Side-coupling, Surface waves, Transmission lines

## 1. Introduction

The characteristic feature of plasmonics is to confine the electromagnetic energy within a sub-wavelength scale far below the diffraction limit [1, 2, 3, 4]. As far as analysis and design of plasmonic structures are concerned, such a strong confinement has two opposite aspects. The negative side is the necessity of going through time-consuming brute-force numerical analysis, which does not impart much physical insight. The positive side is the availability of accurate enough approximate methods based on easy-to-solve distributed circuit networks, which can facilitate the design procedure considerably [5, 6, 7].

Since the planar Metal-Insulator-Metal (MIM) waveguide has been successfully modeled by a simple distributed circuit; viz. a single conductor transmission line [5, 8], much attention is directed toward plasmonic structures that are made of MIM waveguides. Namely, MIM bends [5], splitters [5, 7], demultiplexers [9, 10, 11, 12], stub filters [13, 14, 6], resonators [15, 16], and junctions [13, 17, 18] are all successfully modeled by replacing each waveguide section in the structure with its corresponding single conductor transmission line. Recently, the idea of using single conductor transmission line in modeling of plasmonic structures made of MIM waveguides has been extended to model side coupling between two adjacent single mode MIM waveguides in the structure, e.g. directional coupler, and side coupled waveguide resonator [19, 20]. The extended model is made of two coupled single conductor transmission lines and thus cannot account for the coupling effects that exist among more than two neighboring MIM waveguides. Although the coupling between non-adjacent MIM waveguides is practically negligible, a multi-conductor transmission line model is still needed to analyze structures such as dual-stop-band filters [21], cavity based band-pass filters, and coupled stub configurations.

Here, for the first time to the best of our knowledge, a multi-conductor transmission line with distributed capacitance and inductance matrices is introduced to model the coupling effects that exist among more than two neighboring MIM waveguides. The electrical characteristics of the multi-conductor transmission line in the proposed model are given by closed-form expressions. Thanks to the negligibility of the coupling between non-adjacent MIM waveguides, the per-unit-length capacitance and inductance matrices of the proposed multi-conductor transmission line can be approximated by symmetric tridiagonal matrices [22]. Every diagonal element of the matrix represents the per-unit-length self-capacitance or self-inductance of one of the conductors in the proposed multi-conductor transmission line model. Since each conductor in the model represents one of the coupled MIM waveguides in the structure and since self-coupling effect is reasonably weaker than mutual-coupling effect, the diagonal elements associated with that conductor can be approximately obtained in terms of the per-unit-length self-capacitance and self-inductance of the single conductor transmission line that would represent the same MIM waveguide in the absence of coupling effect. Furthermore, the upper and lower diagonal elements are approximated by the per-unit-length mutual-capacitance and mutual-inductance of the already introduced two coupled single-conductor transmission lines representing the coupling between adjacent MIM waveguides in the structure. The success of the proposed model is indebted to the fact that accurate analysis of side-coupling effects between neighboring MIM structures does not necessitate

consideration of the below cut-off higher order modes. Rather, consideration of the coupling between fundamental modes of the structures, which are represented by the conductor lines of the proposed multi-conductor transmission lines, is usually sufficient. This fact is numerically demonstrated.

This paper is organized as follows: first, the formulation of the proposed multi-conductor transmission line model, its parameters, and its current and voltage distributions, are given by closed-form expressions. The proposed distributed circuit model is then applied to analyze miscellaneous MIM structures, viz. a dual-stop-band filter based on rectangular cavity resonators, a band-pass filter, and MIM waveguide with coupled stubs. The accuracy of the proposed model in all cases is justified by the well-known finite-difference time-domain (FDTD) method. Finally, the conclusions are drawn in section 4.

## 2. Formulation of the proposed model

The schematic view of the considered structure made of $n$ parallel MIM plasmonic waveguides is shown in Fig. 1. The width of the $i$th waveguide is denoted by $w_i$, and the distance between $i$th and $(i+1)$th waveguides is denoted by $d_i$. The permittivity of the dielectric and metallic regions are represented by $\varepsilon_d$, and $\varepsilon_m$, respectively. It is the aim of this section to propose an $n$-conductor transmission line model that accounts for the coupling effects between the $n$ parallel MIM waveguides in the structure. This model is to be applied in analysis of miscellaneous devices in the following sections.

The telegrapher's equations for the $n$-conductor transmission line model read as [23]:

$$\frac{\partial}{\partial z}\mathbf{V} = -j\omega\mathbf{L}\,\mathbf{I} \tag{1a}$$

$$\frac{\partial}{\partial z}\mathbf{I} = -j\omega\mathbf{C}\,\mathbf{V} \tag{1b}$$

where $\omega$ stands for the angular frequency of the harmonic field, $\mathbf{V}$ and $\mathbf{I}$ are voltage and current vectors whose $i$th elements represent transverse electric and magnetic fields of the $i$th MIM waveguide, respectively:

$$\mathbf{V} = \begin{bmatrix} V_1 & V_2 & \dots & V_n \end{bmatrix}^T \tag{2a}$$

$$\mathbf{I} = \begin{bmatrix} I_1 & I_2 & \dots & I_n \end{bmatrix}^T \tag{2b}$$

In these expressions, the per-unit-length inductance; $\mathbf{L} = [L_{ij}]_{n\times n}$, and capacitance; $\mathbf{C} = [C_{ij}]_{n\times n}$, matrices of the $n$-conductor transmission line model are to be found in terms of $w_i$, $d_i$, $\varepsilon_d$, $\varepsilon_m$, and $\omega$. Inasmuch as $\mathbf{L}$ and $\mathbf{C}$ matrices do not vary along the propagation direction; $z$, the voltage and current distributions are given as:

$$\begin{pmatrix}\mathbf{V}\\ \mathbf{I}\end{pmatrix}(z) = \exp(-\mathbf{G}z)\begin{pmatrix}\mathbf{V}\\ \mathbf{I}\end{pmatrix}(0) \tag{3}$$

where

$$\mathbf{G} = j\omega\begin{pmatrix}\mathbf{0}_{n\times n} & \mathbf{L}\\ \mathbf{C} & \mathbf{0}_{n\times n}\end{pmatrix} \tag{4}$$

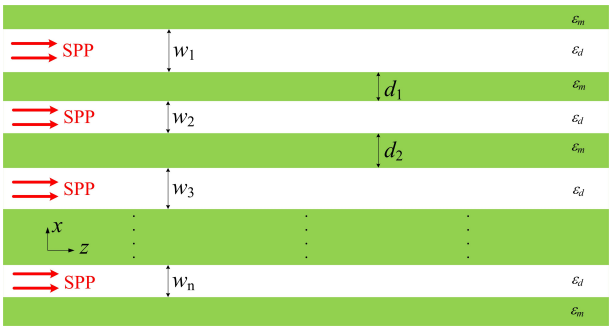


Figure 1: A typical structure made of $n$ side-coupled MIM plasmonic waveguides.

As already mentioned, the coupling effects between nonadjacent waveguides are usually negligible and thus the $n$-conductor transmission line model can be approximated by neglecting $L_{ij}$ and $C_{ij}$ for $|i-j| > 1$. This is schematically shown in Fig. 2, where the self-inductance and the self-capacitance of the $i$th conductor, and the mutual-inductance and the mutual-capacitance between the $i$th and $(i+1)$th conductors are denoted by $L_{\mathrm{s}_i}$, $C_{\mathrm{s}_i}$, $L_{\mathrm{m}_i}$, and $C_{\mathrm{m}_i}$, respectively. Applying Kirchhoff's voltage and current laws proves that the $\mathbf{L}$ and $\mathbf{C}$ matrices in the telegrapher's equations can be approximated by the following tridiagonal matrices:

$$\mathbf{L} \approx \left[L_{\mathrm{s}_i}\delta_{ij} + L_{\mathrm{m}_i}\left(\delta_{i(j+1)} + \delta_{(i+1)j}\right)\right]_{n\times n} \tag{5a}$$

$$\mathbf{C} \approx \left[\left(C_{\mathrm{s}_i} + C_{\mathrm{m}_{(i-1)}} + C_{\mathrm{m}_i}\right)\delta_{ij} - C_{\mathrm{m}_i}\left(\delta_{i(j+1)} + \delta_{(i+1)j}\right)\right]_{n\times n} \tag{5b}$$

in which $\delta_{ij}$ is the kronecker delta:

$$\delta_{ij} = \begin{cases} 1 & \text{if} \quad i = j \\ 0 & \text{if} \quad i \neq j \end{cases} \tag{6}$$

It is worth noting that $L_{\mathrm{s}_i}$ and $C_{\mathrm{s}_i}$ stand for the per-unit-length self-inductance and the self-capacitance of the $i$th conductor in the presence of the coupling between neighboring conductors, and therefore, differ from the per-unit-length self-inductance and the self-capacitance of the $i$th conductor in isolation. Still, the coupling-induced perturbation of $L_{\mathrm{s}_i}$ and $C_{\mathrm{s}_i}$ is weak enough to justify resorting to the closed-form expressions that have been already proposed for an isolated MIM waveguide [19]:

$$C_{\mathrm{s}_i} = \varepsilon_0\varepsilon_d/w_i \tag{7a}$$

$$L_{\mathrm{s}_i} = w_i\,\beta_i^2/(\omega^2\varepsilon_0\varepsilon_d) \tag{7b}$$

where $\beta_i$ is the complex propagation constant of the $i$th MIM waveguide in isolation, and $w_i$ is its width normalized to the unit length in the $y$ direction [7].

Similarly, the coupling-induced perturbation of $L_{\mathrm{m}_i}$, and $C_{\mathrm{m}_i}$ caused by the presence of all other conductors (save the $i$th and $(i+1)$th conductors themselves) can be, to some good extent, neglected and thus the mutual-inductance and the mutual-capacitance between the $i$th and $(i+1)$th conductors can be approximated by resorting to the closed-form expressions that

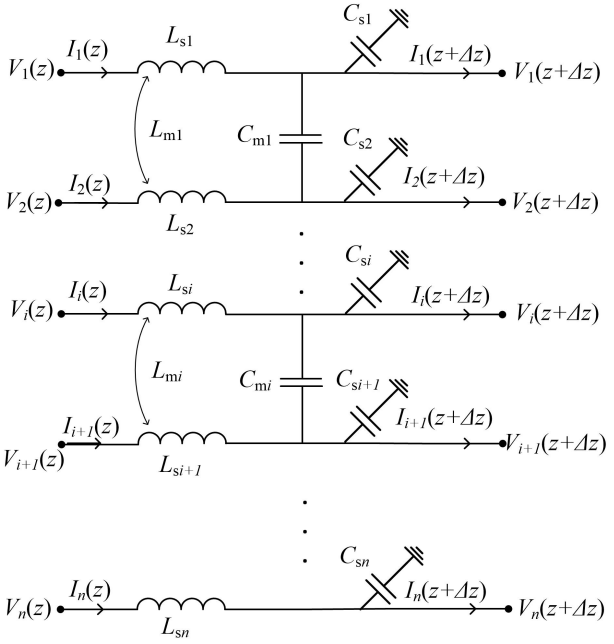


Figure 2: The proposed $n$-conductor transmission line model for the structure in Fig. 1. It is assumed that $L_{ij} = 0$ and $C_{ij} = 0$ for $|i - j| > 1$.

have been already proposed for the mutual-inductance and the mutual-capacitance between two adjacent waveguides [19]:

$$L_{\mathrm{m}_i} = g_{0_i} - \sqrt{g_{0_i}^2 + g_{1_i}} \tag{8a}$$

$$C_{\mathrm{m}_i} = \frac{\beta_{e_i}^2 + \beta_{o_i}^2 - \beta_i^2 - \beta_{i+1}^2}{\omega^2 \left(L_{\mathrm{s}_i} + L_{\mathrm{s}_{(i+1)}} - 2L_{\mathrm{m}_i}\right)} \tag{8b}$$

in which

$$g_{0_i} = \frac{1}{4C_{\mathrm{s}_i}C_{\mathrm{s}_{(i+1)}}}\Big[(C_{\mathrm{s}_i} + C_{\mathrm{s}_{(i+1)}})(\beta_{e_i}^2 + \beta_{o_i}^2)/\omega^2 - L_{\mathrm{s}_i}C_{\mathrm{s}_i}^2 - L_{\mathrm{s}_{(i+1)}}C_{\mathrm{s}_{(i+1)}}^2\Big] - \left(L_{\mathrm{s}_i} + L_{\mathrm{s}_{(i+1)}}\right)/4 \tag{9a}$$

$$g_{1_i} = \frac{(\beta_i\,\beta_{i+1})^2 - (\beta_{e_i}\,\beta_{o_i})^2}{\omega^4\,C_{\mathrm{s}_i}C_{\mathrm{s}_{(i+1)}}} + \frac{L_{\mathrm{s}_i}L_{\mathrm{s}_{(i+1)}}(C_{\mathrm{s}_i} + C_{\mathrm{s}_{(i+1)}})}{C_{\mathrm{s}_i}C_{\mathrm{s}_{(i+1)}}(L_{\mathrm{s}_i} + L_{\mathrm{s}_{(i+1)}})} \times \left(\beta_{e_i}^2 + \beta_{o_i}^2 - \beta_i^2 - \beta_{i+1}^2\right)/\omega^2 \tag{9b}$$

where $\beta_{e_i}$ and $\beta_{o_i}$ denote the propagation constant of the even and odd supermodes in a structure made of the $i$th and $(i + 1)$th MIM waveguides when the rest of the waveguides are absent.

## 3. Applications of the proposed model

The accuracy of the proposed model in analysis of miscellaneous MIM structures, viz. a dual-stop-band filter based on rectangular cavity resonators [21], a band-pass filter based on slot cavity, and MIM waveguide with coupled stubs is numerically shown in this section.

It should be pointed out that all MIM structures including those considered in this manuscript are three-dimensional in practice. Therefore, they are inevitably made of the three-dimensional counterpart of the MIM waveguide, viz. the plasmonic slot waveguide [24, 25, 26]. Fortunately, the plasmonic slot waveguide can be fabricated by using the standard nano-fabrication techniques including electron beam lithography, focused ion milling, and etching processes [24, 27]. It should be also noted that field effect modulation of charge carriers in metal-oxide-silicon (MOS) geometry can successfully imitate MIM waveguides and structures [28, 29]. Therefore, the standard CMOS process can also be employed to realize MIM structures.

The major deviation of the two-dimensional theoretical analysis in this paper from the experimental three-dimensional realization would be due to the out-of-plane leakage from the structure, which is certain to occur at junctions and interfaces, e.g. at bends, stubs, and splitters [24]. The out-of-plane leakage is neglected in this work because the considered structures are two-dimensional and therefore uniform along the out-of-plane direction. Fortunately, the out-of-plane leakage becomes less pronounced at longer wavelengths.

Through out this section, the well-known Drude model [3] is employed for the permittivity of the metallic region:

$$\varepsilon_m(\omega) = \epsilon_\infty - \frac{\omega_p^2}{\omega^2 - j\omega\gamma} \tag{10}$$

The dielectric permittivity is set to $\varepsilon_d = 1$ (the relative permittivity of vacuum), the relative permittivity of silver at very high frequencies is $\epsilon_\infty = 3.7$, the bulk plasma frequency and the collision frequency is respectively set to $\omega_p = 1.38 \times 10^{16}$ Hz, and $\gamma = 2.73 \times 10^{13}$ Hz [30]. The obtained results of the proposed model are justified by two-dimensional FDTD solutions. The FDTD simulations are carried out by using perfectly matched layers (PMLs) boundary conditions and the grid sizes of 2 nm.

### 3.1. Dual-stop-band plasmonic filter

As the first example, a typical dual-stop-band plasmonic filter based on two side-coupled nano cavities (SCNCs) [21] is analyzed by using the proposed model. The schematic of the structure is shown in Fig. 3(a). The widths of the upper SCNC, the waveguide, and the lower SCNC are denoted by $w_1$, $w_2$, and $w_3$ respectively. The coupling length and the distances between the waveguide and the upper and lower SCNCs are denoted by $l$, $d_1$, and $d_2$ respectively.

The corresponding model of this structure is shown in Fig. 3(b). The upper SCNC, the waveguide, and the lower SCNC are each represented by a transmission line whose per-unit-length self-inductance and self-capacitance are denoted by $L_{\mathrm{s}_i}$, and $C_{\mathrm{s}_i}$ ($i$=1, 2, 3), respectively. In accordance with Eq. (7) of the previous section, these per-unit-length circuit elements can be written in terms of the complex propagation constants of the individual MIM waveguides that form the two SCNCs ($\beta_1$ and $\beta_3$) and the middle waveguide of the structure ($\beta_2$). The side coupling between the upper SCNC, the waveguide, and the lower SCNC is modeled by considering the per-unit-length mutual-inductance and mutual-capacitance between the

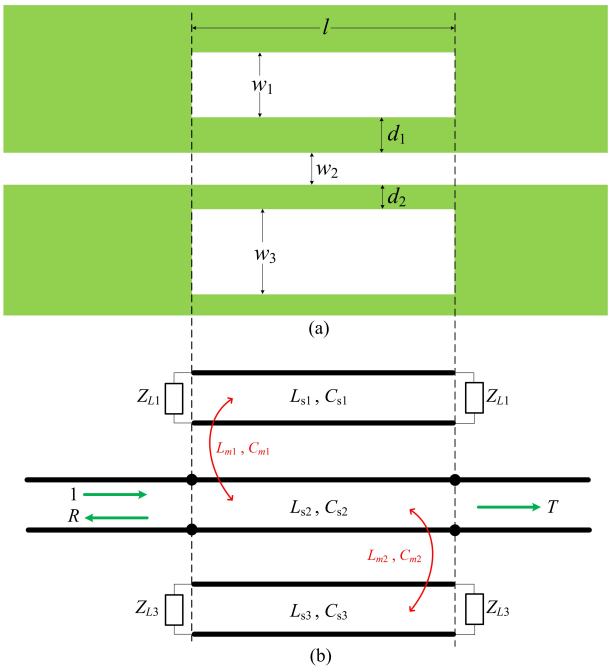


Figure 3: (a) A typical dual-stop-band plasmonic filter based on side-coupled nano cavities (SCNCs). (b) Its corresponding multi-conductor transmission line model.

upper (lower) SCNC, and the waveguide. In accordance with Eqs. (8) and (9) of the previous section, these per-unit-length circuit elements can be written in terms of the complex propagation constants of the even and odd supermodes supported by the coupled MIM waveguides that represent the coupling between the upper (lower) SCNC, and the waveguide. In this fashion, the side-coupling effects are taken into account by a three-conductor transmission line whose per-unit-length inductance, $\mathbf{L}$, and capacitance, $\mathbf{C}$, matrices are as follows:

$$\mathbf{L} \approx \begin{bmatrix} L_{s_1} & L_{m_1} & 0 \\ L_{m_1} & L_{s_2} & L_{m_2} \\ 0 & L_{m_2} & L_{s_3} \end{bmatrix} \tag{11a}$$

$$\mathbf{C} \approx \begin{bmatrix} C_{s_1} + C_{m_1} & -C_{m_1} & 0 \\ -C_{m_1} & C_{m_1} + C_{s_2} + C_{m_2} & -C_{m_2} \\ 0 & -C_{m_2} & C_{s_3} + C_{m_2} \end{bmatrix} \tag{11b}$$

Here, the per-unit-length mutual-inductance and mutual-capacitance between the upper (lower) SCNC, and the waveguide are denoted by $L_{m_1}$ ($L_{m_2}$), and $C_{m_1}$ ($C_{m_2}$), respectively.

As it is shown in Fig. 3(b), the transmission lines that correspond to the upper and lower SCNCs should be of length $l$ and be terminated by appropriate load impedance, $Z_{L_i}$ ($i$=1, 3). Since the complex value of the appropriate load impedance at the terminal ports of the transmission line should comply with the reflection coefficient of the fundamental mode of the MIM waveguide that forms the SCNC, and since that reflection can be accurately approximated by the Fresnel's reflection coefficient [6, 13], $Z_{L_i}$ ($i$=1, 3) can be written as:

$$Z_{L_i} = Z_{w_i} \sqrt{\frac{\varepsilon_d}{\varepsilon_m}} \tag{12}$$

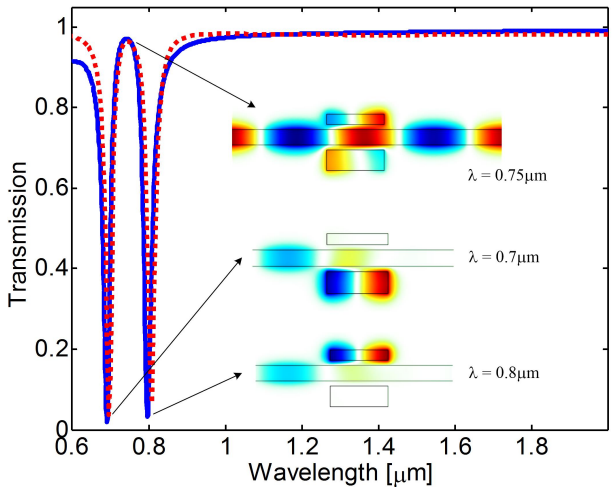


Figure 4: The transmitted power spectrum of the dual-stop-band filter in Fig. 3. The results of the proposed model and of the FDTD are plotted by solid and dotted lines, respectively. Inset shows transverse magnetic field profiles at three different wavelengths.

where $Z_{w_i}$ is the characteristic impedance of the $i$th MIM waveguide [5] and can be written as :

$$Z_{w_i} = w_i \frac{\beta_i}{\omega \varepsilon_0 \varepsilon_d} \tag{13}$$

Now that the parameters of the multi-conductor transmission line model are all given, the reflection; $R$, and transmission; $T$, coefficients of the dual-stop-band plasmonic filter shown in Fig. 3(a) can be easily obtained:

$$T = \det(\mathbf{A_T})/\det(\mathbf{A}) \tag{14a}$$

$$R = \det(\mathbf{A_R})/\det(\mathbf{A}) \tag{14b}$$

where

$$\mathbf{A} = \begin{bmatrix} \mathbf{A_1} & \mathbf{A_2} & \mathbf{A_3} & \mathbf{A_4} & \mathbf{A_5} & \mathbf{A_6} \end{bmatrix} \tag{15a}$$

$$\mathbf{A_T} = \begin{bmatrix} \mathbf{A_1} & \mathbf{b} & \mathbf{A_3} & \mathbf{A_4} & \mathbf{A_5} & \mathbf{A_6} \end{bmatrix} \tag{15b}$$

$$\mathbf{A_R} = \begin{bmatrix} \mathbf{A_1} & \mathbf{A_2} & \mathbf{A_3} & \mathbf{A_4} & \mathbf{b} & \mathbf{A_6} \end{bmatrix} \tag{15c}$$

and

$$\mathbf{A_1} = \begin{pmatrix} Z_{L_1}\mathbf{e_1} \\ \mathbf{e_1} \end{pmatrix}, \ \mathbf{A_2} = \begin{pmatrix} \mathbf{e_2} \\ \mathbf{e_2}/Z_{w_2} \end{pmatrix}, \ \mathbf{A_3} = \begin{pmatrix} Z_{L_3}\mathbf{e_3} \\ \mathbf{e_3} \end{pmatrix} \tag{16a}$$

$$\mathbf{A_4} = \mathbf{E}\begin{pmatrix} Z_{L_1}\mathbf{e_1} \\ -\mathbf{e_1} \end{pmatrix}, \ \mathbf{A_5} = \mathbf{E}\begin{pmatrix} -\mathbf{e_2} \\ \mathbf{e_2}/Z_{w_2} \end{pmatrix}, \ \mathbf{A_6} = \mathbf{E}\begin{pmatrix} Z_{L_3}\mathbf{e_3} \\ -\mathbf{e_3} \end{pmatrix} \tag{16b}$$

$$\mathbf{b} = \mathbf{E}\begin{pmatrix} \mathbf{e_2} \\ \mathbf{e_2}/Z_{w_2} \end{pmatrix}, \ \mathbf{E} = \exp(-\mathbf{G}l) \tag{16c}$$

$$\mathbf{e_1} = \begin{pmatrix} 1 \\ 0 \\ 0 \end{pmatrix}, \ \mathbf{e_2} = \begin{pmatrix} 0 \\ 1 \\ 0 \end{pmatrix}, \ \mathbf{e_3} = \begin{pmatrix} 0 \\ 0 \\ 1 \end{pmatrix} \tag{16d}$$

The accuracy of the above-mentioned expressions for a case where $w_1$ = 50 nm, $w_2$ = 60 nm, $w_3$ = 80 nm, $d_1$ = 20 nm, $d_2$ = 20 nm, and $l$ = 225 nm is shown in Fig. 4, where the transmission coefficient is plotted versus the free space wavelength (solid) and is compared against the FDTD result (dotted).

### 3.2. Plasmonic band-pass filter based on slot cavity

As another example, a typical band-pass plasmonic filter based on a single SCNC is considered. The schematic of the structure is shown in Fig. 5(a). In accordance with the figure, the widths of the upper MIM waveguide, the SCNC, and the lower MIM waveguide are denoted by $w_1$, $w_2$, and $w_3$, respectively. The coupling length between the SCNC and the MIM waveguides is $l_1$ and the length of the SCNC is $l_1 + l_2$. The distance between the SCNC and the upper and lower MIM waveguides are $d_1$, and $d_2$, respectively.

The corresponding model of this structure is shown in Fig. 5(b). The upper and lower MIM waveguides, and the SCNC in their between are each represented by a transmission line whose per-unit-length self-inductance and self-capacitance are denoted by $L_{s_i}$, and $C_{s_i}$ ($i$=1, 2, 3), respectively. Once again, these per-unit-length circuit elements can be written in terms of the complex propagation constants of the individual MIM waveguides that correspond to the upper and lower MIM waveguides and the SCNC of the structure. The side-coupling between the SCNC and the upper and lower MIM waveguides is then modeled by considering the per-unit-length mutual-inductance and mutual-capacitance between the upper (lower) MIM waveguide, and the SCNC. They are respectively denoted by $L_{m_1}$ ($L_{m_2}$), and $C_{m_1}$ ($C_{m_2}$), and can be written in terms of the complex propagation constants of the even and odd supermodes supported by the coupled MIM waveguides that represent the coupling between the upper (lower) MIM waveguide and the SCNC. Much like the previous subsection, the side-coupling effects are taken into account by a three-conductor transmission line whose per-unit-length inductance, $\mathbf{L}$, and capacitance, $\mathbf{C}$, matrices are governed by Eqs. (11a) and (11b).

It is worth noting that the length of the three-conductor transmission line is equal to the coupling length; $l_1$, and differs from the length of the SCNC; $l_1+l_2$. Therefore, the distributed circuit that represents the SCNC is made of two sections. One section is side coupled to the upper and lower MIM waveguides, and is therefore part of the three-conductor transmission line whose length is $l_1$. The other section represents the uncoupled part of the SCNC, and is therefore modeled by a single-conductor transmission line whose length and per-unit-length inductance and capacitance are $l_2$, $L_{s_2}$, and $C_{s_2}$, respectively.

The transmission lines that represent the upper and lower MIM waveguides are terminated at their right-hand-side port by load impedances $Z_{L_1}$, and $Z_{L_3}$, respectively. The transmission line that represents the SCNC is terminated at its both ports by load impedance $Z_{L_2}$. The complex values of the appropriate load impedances can be found by using Eq. (12).

Now that the parameters of the multi-conductor transmission line model are all given, the reflection; $R$, and transmission; $T$, coefficients of the band-pass plasmonic filter shown in Fig. 5(a) can be easily obtained:

$$T = \det(\mathbf{A_T})/\det(\mathbf{A}) \tag{17a}$$

$$R = \det(\mathbf{A_R})/\det(\mathbf{A}) \tag{17b}$$

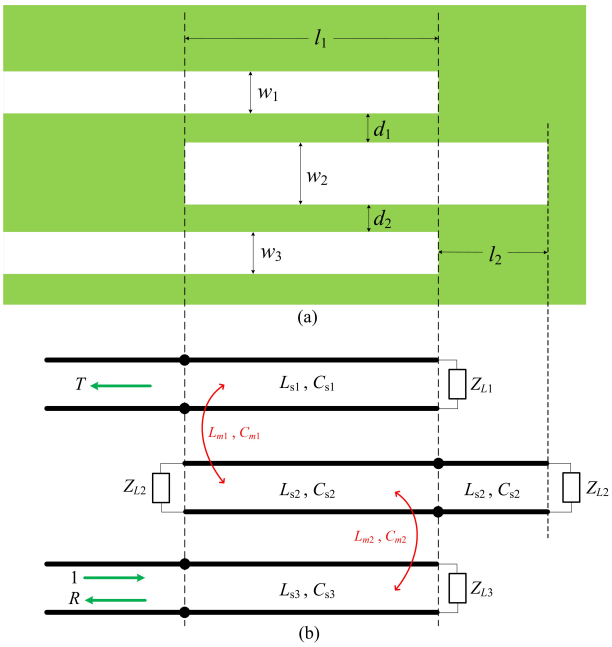


Figure 5: (a) A typical band-pass plasmonic filter based on a side-coupled slot cavity. (b) Its corresponding multi-conductor transmission line model.

where

$$\mathbf{A} = \begin{bmatrix} \mathbf{A_1} & \mathbf{A_2} & \mathbf{A_3} & \mathbf{A_4} & \mathbf{A_5} & \mathbf{A_6} \end{bmatrix} \tag{18a}$$

$$\mathbf{A_T} = \begin{bmatrix} \mathbf{A_1} & \mathbf{A_2} & \mathbf{A_3} & \mathbf{b} & \mathbf{A_5} & \mathbf{A_6} \end{bmatrix} \tag{18b}$$

$$\mathbf{A_R} = \begin{bmatrix} \mathbf{A_1} & \mathbf{A_2} & \mathbf{A_3} & \mathbf{A_4} & \mathbf{b} & \mathbf{A_6} \end{bmatrix} \tag{18c}$$

and

$$\mathbf{A_1} = \begin{pmatrix} Z_{L_1}\mathbf{e_1} \\ \mathbf{e_1} \end{pmatrix}, \ \mathbf{A_2} = \begin{pmatrix} Z_{\text{in}}\mathbf{e_2} \\ \mathbf{e_2} \end{pmatrix}, \ \mathbf{A_3} = \begin{pmatrix} Z_{L_3}\mathbf{e_3} \\ \mathbf{e_3} \end{pmatrix} \tag{19a}$$

$$\mathbf{A_4} = \mathbf{E}\begin{pmatrix} -\mathbf{e_1} \\ \mathbf{e_1}/Z_{w_1} \end{pmatrix}, \ \mathbf{A_5} = \mathbf{E}\begin{pmatrix} -\mathbf{e_3} \\ \mathbf{e_3}/Z_{w_3} \end{pmatrix}, \ \mathbf{A_6} = \mathbf{E}\begin{pmatrix} Z_{L_2}\mathbf{e_2} \\ -\mathbf{e_2} \end{pmatrix} \tag{19b}$$

$$\mathbf{b} = \mathbf{E}\begin{pmatrix} \mathbf{e_3} \\ \mathbf{e_3}/Z_{w_2} \end{pmatrix}, \ Z_{\text{in}} = Z_{w_2}\frac{Z_{L_2} + jZ_{w_2}\tan(\beta_2 l_2)}{Z_{w_2} + jZ_{L_2}\tan(\beta_2 l_2)} \tag{19c}$$

$$\mathbf{e_1} = \begin{pmatrix} 1 \\ 0 \\ 0 \end{pmatrix}, \ \mathbf{e_2} = \begin{pmatrix} 0 \\ 1 \\ 0 \end{pmatrix}, \ \mathbf{e_3} = \begin{pmatrix} 0 \\ 0 \\ 1 \end{pmatrix}, \ \mathbf{E} = \exp(-\mathbf{G}l_1) \tag{19d}$$

The accuracy of the above-mentioned expressions for a band-pass filter tuned at 0.7$\mu$m with parameters $w_1$ = 50 nm, $w_2$ = 50 nm, $w_3$ = 50 nm, $d_1$ = 30 nm, $d_2$ = 30 nm, $l_1$ = 205 nm, and $l_2$ = 0 nm is shown in Fig. 6, where the transmission coefficient is plotted versus the free space wavelength (solid) and is compared against the FDTD result (dotted).

### 3.3. Plasmonic stub filter

Without losing generality, a typical plasmonic stub filter made of an MIM waveguide of width $w_3$, and two stubs of widths $w_1$, and $w_2$ is considered. Fig. 7(a) shows the schematic view of this structure. The lengths of the first and second stubs are $h + \Delta h$, and $h$, respectively. The distance between the two stubs is denoted by $d_0$.

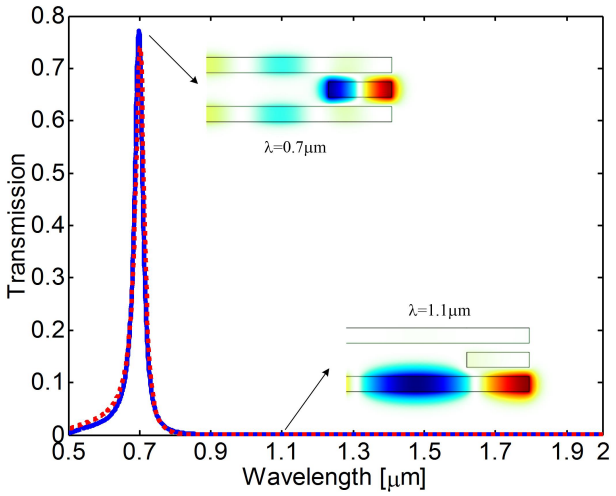


Figure 6: The transmitted power spectrum of the band-pass filter in Fig. 5. The results of the proposed model and of the FDTD are plotted by solid and dotted lines, respectively. Inset shows transverse magnetic field profiles at two different wavelengths.

The corresponding model of this structure is shown in Fig. 7(b). The MIM waveguide is modeled by a single conductor transmission line whose per-unit-length circuit elements are denoted by $L_{s_3}$ and $C_{s_3}$. The terminations of the two stubs are modeled by complex load impedances; $Z_{L_1}$ and $Z_{L_2}$. It is worth noting that $Z_{L_1}$, $Z_{L_2}$, $L_{s_3}$ and $C_{s_3}$ are all already given [see Eqs. (7) and (12)]. In the conventional transmission line model [13], the first and second stubs are modeled by two uncoupled single-conductor transmission lines of length $h + \Delta h$, and $h$, respectively. The per-unit-length self-inductance and self-capacitance of these two transmission lines; $L_{s_i}$ and $C_{s_i}$ ($i = 1, 2$), are determined in terms of the propagation constants and widths of the MIM waveguides that form the stub sections. What makes the proposed model different from the conventional transmission line model is that the coupling between the neighboring stubs is no longer neglected. This could be a matter of consequence when $d_0$ is small enough to cause a strong coupling.

To include the coupling effects in the proposed model, the per-unit-length mutual inductance, $L_{m_1}$, and mutual capacitance, $C_{m_1}$, between the hitherto uncoupled single-conductor transmission lines that represent the stub sections are taken into account. Much like the previous subsections, these per-unit-length mutual circuit elements can be found in terms of the complex propagation constants of the even and odd supermodes. These supermodes are supported by the coupled MIM waveguides that represent the coupling between the neighboring stubs. In this manner, the first and second stubs are modeled together; even though the extra length of the first stub is left to be modeled by a single conductor transmission line of length $\Delta h$. Evidently, the per-unit-length self-inductance and self-capacitance of this single-conductor transmission line are $L_{s_1}$ and $C_{s_1}$.

Two numerical examples are given. First, it is assumed that $w_1 = 50$ nm, $w_2 = 50$ nm, $w_3 = 50$ nm, $h = 300$ nm, $\Delta h = 0$ nm, and $d_0 = 100$ nm. The transmission coefficient of the structure is obtained by using the proposed circuit model and the FDTD method. The obtained results are plotted versus the free space wavelength in Fig. 8(a). It is worth noting that the results of the proposed model and the conventional model [13] where the coupling effects are neglected virtually overlap. Second, the distance between the neighboring stubs in the same structure is decreased to $d_0 = 20$ nm. The transmission coefficient of the structure is once again obtained by using the proposed circuit model, the conventional transmission line model [13], and the FDTD method. The obtained results are plotted versus the free space wavelength in Fig. 8(b). This time, the results of the conventional approach differ from the results of the proposed model. Since the latter is more close to the FDTD results,

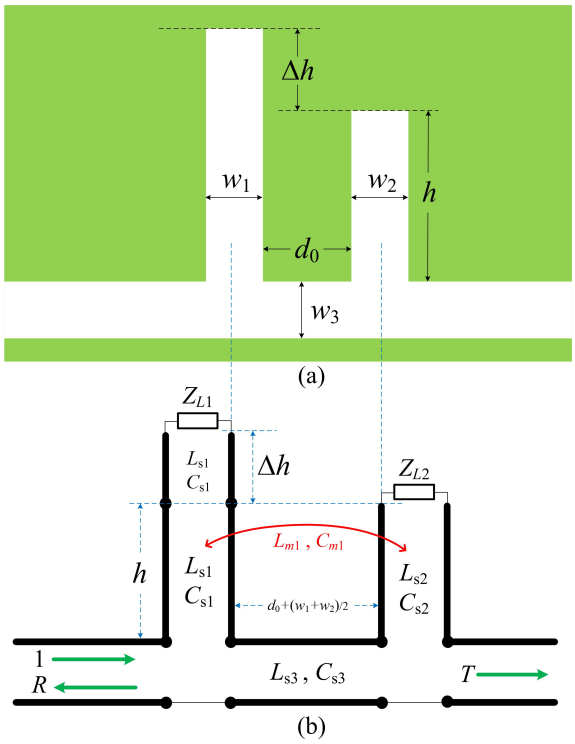


Figure 7: (a) A typical MIM plasmonic structure with two neighboring stubs. (b) Its corresponding multi-conductor transmission line model.

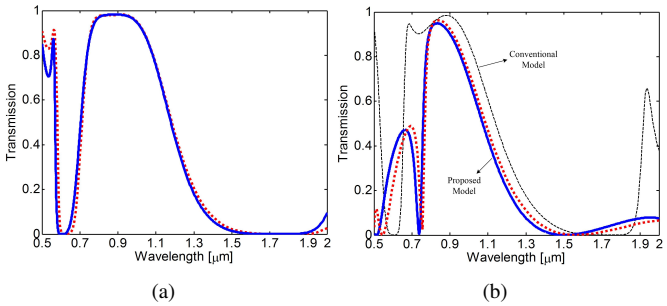


Figure 8: The transmitted power spectrum of the structure in Fig. 7 when (a) $d_0 = 100$ nm and the coupling is weak, and (b) $d_0 = 20$ nm and the coupling is strong. The results of the proposed multi-conductor transmission line model, of the conventional transmission line model, and of the FDTD method are plotted by solid, dashed, and dotted lines respectively.

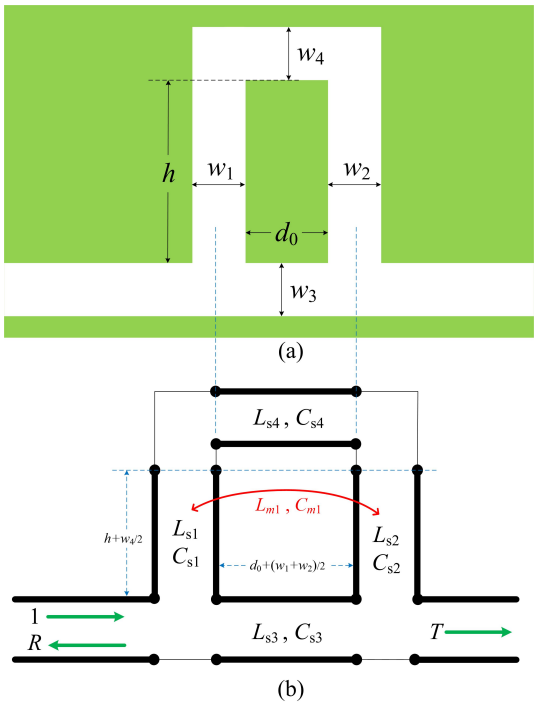


Figure 9: (a) The structure of a plasmonic loop feedback. (b) The proposed transmission line model for analyzing the structure.

the coupling effects should be included, particularly at shorter wavelengths.

### *3.4. Plasmonic feedback configuration*

Finally, a recently proposed structure having a plasmonic feedback loop [31] is considered . The schematic view of this structure is shown in Fig. 9(a). The corresponding multi-conductor transmission line model of this structure is shown in Fig. 9(b). It is not dissimilar to the multi-conductor transmission line model of the structure in Fig. 7. Only this time the two conductors of the transmission line model representing the coupled stub sections are not terminated by complex load impedances. Rather, they are connected to each other via a single conductor transmission line whose per-unit-length self-inductance and self-capacitance; $L_{s_4}$ and $C_{s_4}$, depend on the propagation constant and width of the MIM waveguide that forms the upper side of the square feedback loop.

As an example, it is assumed that $h$ = 200 nm, $d_0$ = 20 nm, $w_1$ = 50 nm, $w_2$ = 50 nm, $w_3$ = 50 nm, and $w_4$ = 50 nm. The transmission coefficient of the structure is obtained by using the proposed circuit model and the FDTD method. The obtained results are plotted versus the free space wavelength in Fig. 10. They are in very good agreement with each other.

## 4. Conclusion

In this paper, a multi-conductor transmission line model was proposed for miscellaneous side-coupled MIM plasmonic structures. Closed-form expressions were given for the parameters of the proposed model. The accuracy of the proposed model was assessed by using the FDTD method. It was

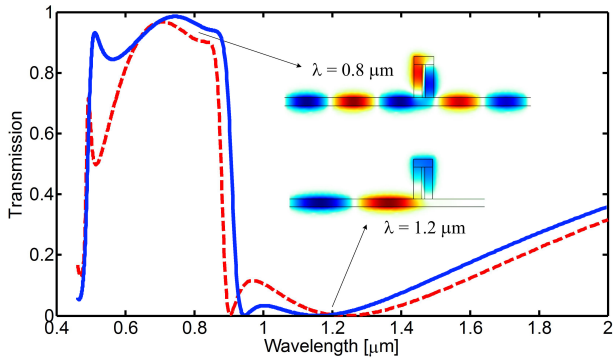


Figure 10: The transmitted power spectrum of the structure with square loop feedback in Fig. 9. The results of the proposed model and of the FDTD are plotted by solid and dashed lines, respectively. Inset shows the transverse magnetic field profile at $\lambda$ = 0.8 and 1.2 $\mu$m.

shown that the proposed model is capable of providing accurate enough results. The results of the proposed model can be obtained at almost no computational cost.

It is worth noting that the proposed model is also applicable to non-plasmonic structures whenever the electromagnetic energy is highly confined, i.e. whenever the higher order modes are below cut-off and thus do not play a critical role. One noticeable example is the possibility of applying our method to photonic crystal based devices and structures. Interestingly, every single example in this manuscript has a photonic crystal counterpart, which can be successfully modeled by similar multi-conductor transmission lines. Although there have been some efforts to model photonic crystal structures via single conductor transmission line models [32, 33, 34, 35, 36], the idea of using multi-conductor transmission lines has never been applied to photonic crystal structures.

## References


[1] S. Maier, Plasmonics: The promise of highly integrated optical devices, Selected Topics in Quantum Electronics, IEEE Journal of 12 (6) (2006) 1671–1677.

[2] D. K. Gramotnev, S. I. Bozhevolnyi, Plasmonics beyond the diffraction limit, Nature Photonics 4 (2) (2010) 83–91.

[3] S. Maier, Plasmonics: fundamentals and applications, Springer, 2007.

[4] S. I. Bozhevolnyi, Plasmonic nano-guides and circuits, in: Plasmonics and Metamaterials, Optical Society of America, 2008.

[5] G. Veronis, S. Fan, Bends and splitters in metal-dielectric-metal subwavelength plasmonic waveguides, Applied Physics Letters 87 (13) (2005) 131102–131102.

[6] A. Pannipitiya, I. D. Rukhlenko, M. Premaratne, H. T. Hattori, G. P. Agrawal, Improved transmission model for metal-dielectric-metal plasmonic waveguides with stub structure, Optics Express 18 (6) (2010) 6191–6204.

[7] H. Nejati, A. Beirami, Theoretical analysis of the characteristic impedance in metal–insulator–metal plasmonic transmission lines, Optics Letters 37 (6) (2012) 1050–1052.

[8] M. Staffaroni, J. Conway, S. Vedantam, J. Tang, E. Yablonovitch, Circuit analysis in metal-optics, Photonics and Nanostructures-Fundamentals and Applications 10 (1) (2012) 166–176.

[9] M. Bahadori, A. Eshaghian, H. Hodaei, M. Rezaei, K. Mehrany, Analysis and design of optical demultiplexer based on arrayed plasmonic slot cavities: Transmission line model, Photonics Technology Letters, IEEE 25 (8) (2013) 784–786.

[10] N. Nozhat, N. Granpayeh, Analysis of the plasmonic power splitter and mux/demux suitable for photonic integrated circuits, Optics Communications 284 (13) (2011) 3449–3455.
[11] F. Hu, H. Yi, Z. Zhou, Wavelength demultiplexing structure based on arrayed plasmonic slot cavities, Optics letters 36 (8) (2011) 1500–1502.
[12] Y. Guo, L. Yan, W. Pan, B. Luo, K. Wen, Z. Guo, H. Li, X. Luo, A plasmonic splitter based on slot cavity, Optics Express 19 (15) (2011) 13831–13838.
[13] A. Pannipitiya, I. Rukhlenko, M. Premaratne, Analytical modeling of resonant cavities for plasmonic-slot-waveguide junctions, Photonics Journal, IEEE 3 (2) (2011) 220–233.
[14] Y. Matsuzaki, T. Okamoto, M. Haraguchi, M. Fukui, M. Nakagaki, Characteristics of gap plasmon waveguide with stub structures, Optics Express 16 (21) (2008) 16314–16325.
[15] Q. Zhang, X. Huang, X. Lin, J. Tao, X. Jin, A subwavelength coupler-type mim optical filter, Optics express 17 (9) (2009) 7549–7555.
[16] M. Rezaei, M. Miri, A. Khavasi, K. Mehrany, B. Rashidian, An efficient circuit model for the analysis and design of rectangular plasmonic resonators, Plasmonics 7 (2) (2012) 245–252.
[17] G. Veronis, S. E. Kocabas, D. A. Miller, S. Fan, Modeling of plasmonic waveguide components and networks, Journal of Computational and Theoretical Nanoscience 6 (8) (2009) 1808–1826.
[18] H. Hodaei, M. Rezaei, M. Miri, M. Bahadori, A. Eshaghian, K. Mehrany, Easy-to-design nano-coupler between metal–insulator–metal plasmonic and dielectric slab waveguides, Plasmonics 8 (2013) 1123–1128.
[19] M. Rezaei, S. Jalaly, M. Miri, A. Khavasi, A. Fard, K. Mehrany, B. Rashidian, A distributed circuit model for side-coupled nanoplasmonic structures with metal–insulator–metal arrangement, Selected Topics in Quantum Electronics, IEEE Journal of 18 (6) (2012) 1692–1699.
[20] M. Bahadori, A. Eshaghian, M. Rezaei, H. Hodaei, K. Mehrany, Coupled transmission line model for planar metal-dielectric-metal plasmonic structures: inclusion of the first non-principal mode, Quantum Electronics, IEEE Journal of 49 (9) (2013) 777–784.
[21] H. Lu, X. Liu, L. Wang, D. Mao, Y. Gong, Nanoplasmonic triple-wavelength demultiplexers in two-dimensional metallic waveguides, Applied Physics B 103 (4) (2011) 877–881.
[22] W. Barth, R. Martin, J. Wilkinson, Calculation of the eigenvalues of a symmetric tridiagonal matrix by the method of bisection, Numerische Mathematik 9 (5) (1967) 386–393.
[23] D. Pozar, Microwave engineering, John Wiley & Sons, 2009.
[24] W. Cai, W. Shin, S. Fan, M. L. Brongersma, Elements for plasmonic nanocircuits with three-dimensional slot waveguides, Advanced materials 22 (45) (2010) 5120–5124.
[25] G. Veronis, S. Fan, Modes of subwavelength plasmonic slot waveguides, Journal of Lightwave Technology 25 (9) (2007) 2511–2521.
[26] Z. Han, A. Elezzabi, V. Van, Experimental realization of subwavelength plasmonic slot waveguides on a silicon platform, Optics letters 35 (4) (2010) 502–504.
[27] J. Dionne, H. Lezec, H. A. Atwater, Highly confined photon transport in subwavelength metallic slot waveguides, Nano Letters 6 (9) (2006) 1928–1932.
[28] J. A. Dionne, K. Diest, L. A. Sweatlock, H. A. Atwater, Plasmostor: a metal- oxide- si field effect plasmonic modulator, Nano Letters 9 (2) (2009) 897–902.
[29] J. Dionne, L. Sweatlock, M. Sheldon, A. Alivisatos, H. Atwater, Silicon-based plasmonics for on-chip photonics, Selected Topics in Quantum Electronics, IEEE Journal of 16 (1) (2010) 295–306.
[30] J. Tao, X. Huang, X. Lin, Q. Zhang, X. Jin, A narrow-band subwavelength plasmonic waveguide filter with asymmetrical multiple-teeth-shaped structure, Optics express 17 (16) (2009) 13989–13994.
[31] M. Swillam, A. Helmy, Feedback effects in plasmonic slot waveguides examined using a closed form model, Photonics Technology Letters, IEEE 24 (6) (2012) 497–499.
[32] M. Miri, A. Khavasi, M. Miri, K. Mehrany, A transmission line resonator model for fast extraction of electromagnetic properties of cavities in two-dimensional photonic crystals, Photonics Journal, IEEE 2 (4) (2010) 677–685.
[33] A. Khavasi, M. Rezaei, M. Miri, K. Mehrany, Circuit model for efficient analysis and design of photonic crystal devices, Journal of Optics 14 (12) (2012) 125502.
[34] N. Habibi, A. Khavasi, M. Miri, K. Mehrany, Circuit model for mode extraction in lossy/lossless photonic crystal waveguides, JOSA B 29 (1) (2012) 170–177.
[35] A. Khavasi, M. Miri, M. Rezaei, K. Mehrany, B. Rashidian, Transmission line model for extraction of transmission characteristics in photonic crystal waveguides with stubs: optical filter design, Optics Letters 37 (8) (2012) 1322–1324.
[36] N. Nozhat, R. McPhedran, C. de Sterke, N. Granpayeh, The plasmonic folded directional coupler, Photonics and Nanostructures-Fundamentals and Applications 9 (4) (2011) 308–314.